---

**Article:**
Lu, Z., Sinclair, D.C. orcid.org/0000-0002-8031-7678 and Reaney, I.M. orcid.org/0000-0003-3893-6544 (2015) The Influence of La Doping and Heterogeneity on the Thermoelectric Properties of Sr3Ti2O7 Ceramics. Journal of the American Ceramic Society, 99 (2). pp. 515-522. ISSN 0002-7820

https://doi.org/10.1111/jace.13998

---

# The influence of La-doping and heterogeneity on the thermoelectric properties of $Sr_3Ti_2O_7$ ceramics.

Zhilun Lu[1], Derek C. Sinclair[1], Ian M. Reaney[1*]

Department of Materials Science & Engineering, University of Sheffield, Sheffield, S1 3JD, UK

*Corresponding Author's e-mail: i.m.reaney@sheffield.ac.uk

## Abstract

La-doping mechanisms and thermoelectric properties of $Sr_3Ti_2O_7$ Ruddlesden-Popper (RP) ceramics sintered under air and flowing 5% $H_2$ at 1773 K for 6 hours have been investigated. Changes in lattice parameters and conductivity revealed a limited interstitial anion mechanism (~1 at.%) based on $La^{3+} + ½O^{2-} \rightarrow Sr^{2+}$ which resulted in insulating samples when processed in air. In contrast, electronic donor-doping ($La^{3+} + e^- \rightarrow Sr^{2+}$) and oxygen loss [$O^{2-} \rightarrow ½ O_2$ (g) + 2 $e^-$] are the dominant mechanism(s) in 5% $H_2$-sintered ceramics with a solution limit of ~5 at.%. The increased solubility limit is attributed to the formation of $Ti^{3+}$ during reduction which compensates for the extra positive charge associated with La on the A-site and also to the occurrence of oxygen loss due to the reducing conditions. For 5% $H_2$-sintered samples, an insulating surface layer formed associated with SrO volatilisation and oxygen up-take (during cooling) from the sintering. Unless removed, the insulating layer masked the conductive nature of the ceramics. In the bulk, significantly higher power factors were obtained for ceramics that

were phase mixtures containing highly conductive perovskite-based (Sr,La)$TiO_{3-\delta}$ (ST). This highlights the superior power factor properties of reduced perovskite-type ST phases compared to reduced RP-type $Sr_3Ti_2O_7$ and serves as a precaution for the need to identify low levels of highly conducting perovskite phases when exploring rare-earth doping mechanisms in RP-type phases.

## I. Introduction

Considerable research activity in the field of thermoelectric materials has taken place in recent years due to their ability to directly convert heat into electricity. The performance of a thermoelectric device is characterised by the dimensionless figure-of-merit ZT, which is defined as, $ZT = S^2\sigma T/\kappa$, where S is the Seebeck coefficient, $\sigma$ is the electrical conductivity, $\kappa$ is the thermal conductivity and T is the average temperature in Kelvin. Large ZT values for state-of-the-art thermoelectrics have been obtained in antimony-[1], tellurium-[2], and germanium-[3]based compounds, which are made up of toxic, rare elements that melt easily at high temperatures in air[4]. Thus, oxide materials are promising candidates for high-temperature thermoelectric applications based on their potential nontoxicity, natural abundance, durability, cheapness and high thermal stability[5-7].

ZT is typically optimised due to a combination of high $\sigma$ and S coupled with low $\kappa$. Strontium titanate, (ST) with a simple cubic perovskite structure is a good n-type thermoelectric material based on its prominent $\sigma$ by doping higher valence donor ions on the A- and B-site and the high effective mass of the carriers. For example, heavily donor-

doped (electronic) ST with $La^{3+}$ and $Nb^{5+}$, show power factors (PF = $S^2\sigma$) of ~800[8] and 1300 μW/m/$K^2$ at 1000 K[9], respectively. In addition to chemical doping, removal of lattice oxygen by processing ST materials in reducing atmospheres (e.g., 5% $H_2$ at >1473 K) is another effective method to increase carrier concentration, Eq. (1).

$$O_O^x \rightarrow V_O^{\bullet\bullet} + 2e' + 1/2\ O_2(g) \quad (1)$$

These materials have high σ and large S which are sufficient to compete with conventional thermoelectric materials[10]. Unfortunately, κ is high (~10 W/m/K at 300 K) due to the lack of effective phonon-scattering centres in the simple cubic perovskite structure, even with the presence of cation dopants and/or oxygen vacancies as defects.

To promote lower κ in perovskite-type phases requires a lowering of crystal symmetry to shorten the mean free path of the phonons and this can be achieved by exploring Ruddlesden-Popper (RP) phases as opposed to cubic perovskites. The perovskite layers of doped and reduced RP phases should retain high σ without significantly suppressing S but disruption of octahedral phonon modes across successive perovskite blocks separated by Rock Salt (RS) layers can reduce κ compared with conventional $ABO_3$ perovskites. Based on the best thermoelectric properties obtained in Nb-doped $SrTiO_3$, the thermoelectric properties of RP phases have been studied for Nb-doped compounds prepared in an inert atmosphere by Lee et al., where they reported a highest PF of ~300 μW/m/$K^2$ at 1000 K for $Sr_3Ti_{1.95}Nb_{0.05}O_7$[11]. They extended their research to A-site doped RP phases and reported a PF ~430 μW/m/$K^2$ at 1000 K for 5 at. % La-doped $Sr_3Ti_2O_7$[12, 13] and achieved a maximum PF (~450 μW/m/$K^2$ at 1000 K) for $(Sr_{0.95}Gd_{0.05})_3Ti_2O_7$[14, 15]. The lower PF values compared to ST perovskites was primarily due to the lower σ of the RP phases containing insulating RS layers between the

perovskite blocks and this has been proposed to be the main obstacle in the development of good thermoelectric properties in RP phases[16]. However, these materials were prepared in inert atmospheres and therefore the influence of reduction from mechanism (1) on σ has not been investigated.

The electronic or so-called 'donor-doping' mechanism in Eq. (2) has been widely used to create free electrons in the lattice to increase σ of La-doped $SrTiO_3$ and $Sr_3Ti_2O_7$[13, 14, 17-19]. However, there are at least three compensation mechanisms in La-doped $SrTiO_3$, which can also be dependent on the conditions of synthesis, e.g., $P_{O_2}$ and temperature[20-22]. These are listed as mechanisms (2)-(4) and represent electronic, A-site and B-site vacancies, respectively. In the case of RP phases there is a further possibility of oxygen interstitials, as shown in mechanism (5). Note that the cation compositions for mechanisms (2) and (5) are identical; however, samples based on mechanism (2) are generally good n-type electronic conductors whereas those based on mechanism (5) can have various properties ranging from insulating, mixed ionic/electronic to ionic ($O^{2-}$) conductors[23].

$$Sr^{2+} \rightarrow La^{3+} + e^- \quad (2)$$

$$3Sr^{2+} \rightarrow 2La^{3+} \quad (3)$$

$$Sr^{2+} + ¼\ Ti^{4+} \rightarrow La^{3+} \quad (4)$$

$$Sr^{2+} \rightarrow La^{3+} + ½O^{2-} \quad (5)$$

Improvement of σ for La-doped $Sr_3Ti_2O_7$ under inert atmospheres may predominantly be a consequence of mechanism (2) and possibly some oxygen loss [mechanism (1)] in the process of ceramic preparation.

To clarify the influence of reducing conditions on the La-doping mechanism(s) and PF properties of the RP phase $Sr_3Ti_2O_{7,}$ we present results for ceramics based on the La-doping mechanisms listed above prepared in ambient (air) and reducing (5% $H_2$) atmospheres. Furthermore, we highlight the influence of heterogeneity associated with resistive surface layers and conductive secondary phases on the electrical properties of ceramics processed under reducing atmospheres. Recognition of these heterogeneities is important as processing titanate-based ceramics under reducing conditions is a common method to induce significant levels of oxygen-loss, mechanism (1), and therefore n-type conduction in these materials.

## II. Experimental

$(Sr_{1-x}La_x)_3Ti_2O_7$, $(Sr_{1-3y/2}La_y)_3Ti_2O_7$ and $(Sr_{1-z}La_z)_3Ti_{2-3z/4}O_7$ ceramics (from 0 to 0.10) were prepared from $SrCO_3$ (99.90%, Sigma Aldrich), $La_2O_3$ (99.99%, Sigma Aldrich) and $TiO_2$ (99.90%, Sigma Aldrich) by a solid state reaction method. Stoichiometric amounts of dry raw materials (drying temperatures of 573 K ($SrCO_3$), 1173 K ($TiO_2$ and $La_2O_3$) were weighed with a precision of ± 0.0001 g. Starting powders were mixed using an attrition mill for 60 minutes with yttria-stabilised zirconia (YSZ) media in iso-propanol. After being dried at ~353 K and sieved through a 300 μm mesh, mixed powders were calcined at 1473 K for 12 hours in an alumina crucible to decompose the carbonate and homogenise the reactants. Pellets and bar samples were prepared using a uniaxial press with calcined powders in a square die, followed by cold isostatic pressing at 200 MPa and finally sintering in air or flowing 5% $H_2$-95% $N_2$ gas (referred to as 5 % $H_2$ forthwith) at 1773 K for 6 h, respectively.

A high resolution STOE STADI-P diffractometer (STOE & Cie GmbH, Darmstadt, Germany) with a linear position sensitive detector (PSD) was used for crushed samples with CuKα (λ = 1.5406 Å) radiation. The operating voltage and current were 40 kV and 30 mA, respectively. Ceramic microstructure was examined using an FEI Inspect F Scanning Electron Microscope (SEM) and JEOL JEM 3010 Transmission Electron Microscopy (TEM). All SEM samples were carbon-coated prior to examination.

Impedance spectroscopy (IS) was performed on an Agilent E4980A over a frequency range of 20 Hz-2 MHz with an applied voltage of 100 mV using In/Ga electrodes. S and σ were measured simultaneously on ~20×3×3 mm bar samples with Ag

electrodes by a conventional steady state method and a four-probe method, respectively, in air from 473 to 973 K.

## III. Results

### (1) La-Doped $Sr_3Ti_2O_7$ Ceramics Sintered in Air

All doped samples (irrespective of x, y or z) prepared in air were off-white in appearance and with the exception of x = 0.01 all were confirmed as phase mixtures by a combination of XRD (not shown) and analytically electron microscopy. Secondary phases identified included a perovskite-type $SrTiO_3$ for x and y and B-site deficient hexagonal-type perovskite $SrLa_4Ti_4O_{15}$ and an anion-excess layered-type perovskite $SrLa_4Ti_5O_{17}$ for z. Identifying low levels of perovskite-type $SrTiO_3$ as a secondary phase was challenging for the x series but was confirmed in x = 0.02 and 0.05 by the appearance of an additional reflection in the XRD patterns at ~$40^o$ two theta (hkl = 111) Fig. 1(a) and was also observed by TEM (discussed later). The XRD pattern for powder of x = 0.01 crushed pellets fully indexed to $Sr_3Ti_2O_7$ ([11-633] ICDD card) and there was an expansion of the unit cell volume compared to undoped $Sr_3Ti_2O_7$ prepared in air, Fig. 1(b). The high frequency arc in impedance complex plane, Z*, plots was used to extract the bulk (grain) resistivity, ($\rho_b$) of undoped $Sr_3Ti_2O_7$ and x = 0.01 ceramics sintered in air. The bulk conductivity, $\sigma_b = 1/\rho_b$, plotted in Arrhenius-format shows the La-doped ceramics to have lower conductivity (~1 to 1.5 orders of magnitude at ~893 K) and a significantly higher activation energy for bulk conduction, $E_a$, (~1 eV) compared to undoped $Sr_3Ti_2O_7$, Fig. 2.

### (2) Undoped $Sr_3Ti_2O_{7-\delta}$ Ceramics Sintered in 5% $H_2$

The colour of undoped $Sr_3Ti_2O_7$ ceramics sintered in 5% $H_2$ ($Sr_3Ti_2O_{7-\delta}$) was dark green suggesting oxygen-loss with partial reduction of $Ti^{4+}$ to $Ti^{3+}$ ions had occurred within the

ceramics. This was in contrast to the off-white colour with fully oxidised $Ti^{4+}$ ions for undoped $Sr_3Ti_2O_7$ ceramics prepared in air. XRD performed on the surface of undoped $Sr_3Ti_2O_{7-\delta}$ ceramics sintered in 5% $H_2$ and on powder from crushed pellets gave very different results, Fig. 3. The XRD pattern for the powder of crushed pellets fully indexed to $Sr_3Ti_2O_7$ ([11-633] ICDD card) but with considerable expansion of unit cell volume when compared to undoped ceramics prepared in air, Fig. 1(b). In contrast, the XRD pattern for the ceramic surface contained many additional reflections. Some of these are associated with a simple $SrTiO_3$-type cell (presumably oxygen-deficient and referred forthwith as $SrTiO_{3-\delta}$ due to the high temperature and low $pO_2$ employed during the synthesis), however, there are other reflections that do not index to any known phase in the ICDD database.

Backscattered electron images (BEI) on a cross section of a pellet sintered in 5% $H_2$ are shown in Fig. 4. The BEI demonstrated clear evidence for the presence of a surface layer with a different composition to that of the ceramic interior. EDS analysis showed the Sr/Ti ratio to be lower for the surface layer (Sr/Ti ~ 1) compared to the interior of the ceramic (Sr/Ti ~ 3/2), Table 1.

Typical Z* plots at RT for unpolished and polished $Sr_3Ti_2O_{7-\delta}$ ceramics sintered in 5% $H_2$ were dramatically different, Fig. 5. A Z* plot for an unpolished ceramic was dominated by a single, large arc that could not be fully resolved as the total resistivity of the sample exceeded >10 MΩcm, Fig. 5(a). In contrast, the Z* plot for the polished pellet showed a single arc with a total sample resistivity of ~40 kΩcm at RT, Fig. 5(b). This showed the as-sintered ceramic to contain a resistive surface layer. Using the relationship $\omega RC = 1$ at the arc maximum in Fig. 5(b) showed the associated Capacitance, C, of this

arc to be 173 μF/cm, consistent with non-ohmic contacts between the polished ceramic and the metal electrodes. The size of this arc changed with the application of a small dc bias (<2 V) to the IS measurements and also when changing the work-function of the metal electrode by replacing In/Ga electrodes with Ag (not shown). These observations support the assignment of this arc to non-ohmic electrode contacts. Inspection of high frequency data in the RT Z* plot showed the presence of a non-zero intercept of ~4 Ωcm associated with the total resistivity of the ceramic, Fig. 5(c). Cryogenic measurements were performed in an attempt to quantify the bulk (grain) response via the presence of a high frequency Debye peak in the imaginary component of the electric modulus M″ spectrum[24, 25]. A combined -Z″ and M″ spectroscopic plot at 10 K showed a low frequency -Z″ Debye peak associated with the resistive, non-ohmic contact, however, the M″ spectrum showed an incline at high frequency indicating the grain (bulk) response remained too conductive to measure by IS, Fig. 5(d) at 10 K. The M″ Debye peak at intermediate frequency is attributed to a thin layer (electrode/surface) response, Fig. 5(d) but was not investigated in detail.

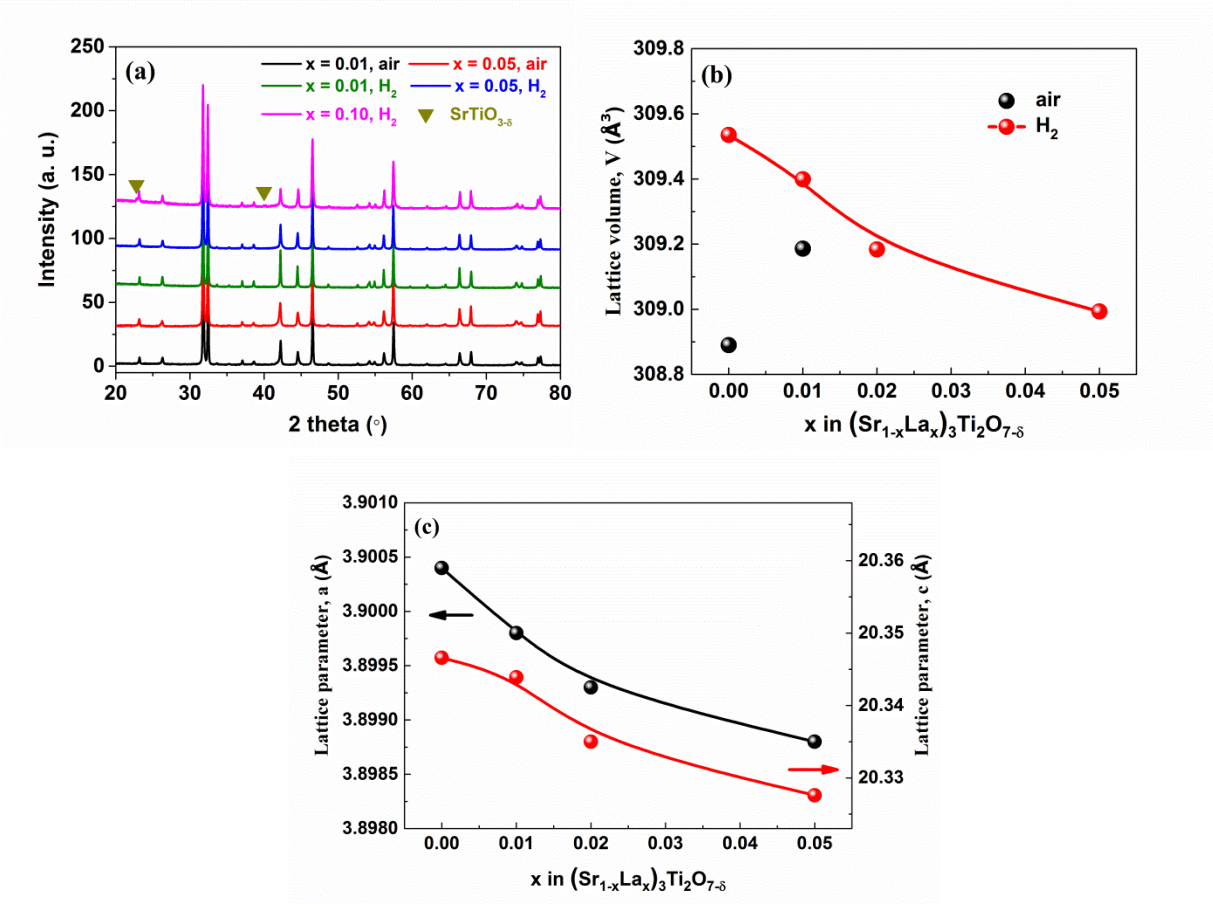


**Fig. 1.** (a) XRD patterns for $(Sr_{1-x}La_x)_3Ti_2O_7$ ceramics sintered in air and 5% $H_2$, (b) unit cell volume for x-series ceramics sintered in air (black filled circles) and 5% $H_2$ (red filled circles), and (c) lattice parameters for $(Sr_{1-x}La_x)_3Ti_2O_{7-\delta}$ ceramics sintered in 5% $H_2$.

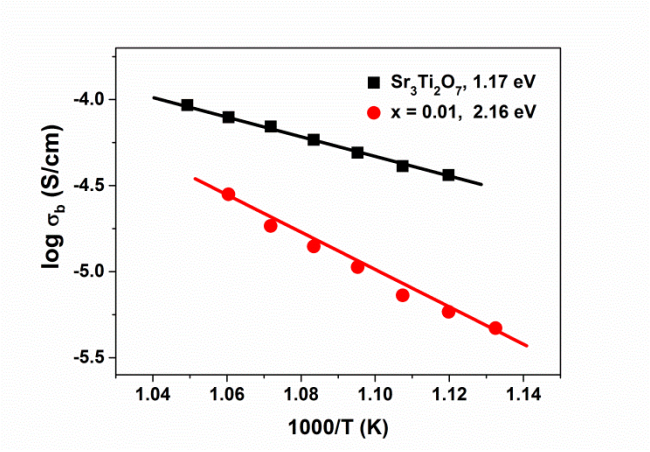


**Fig. 2.** Arrhenius plots of $\sigma_b$ for undoped $Sr_3Ti_2O_7$ (filled black squares) and x = 0.01 (filled red circles) ceramics sintered in air.

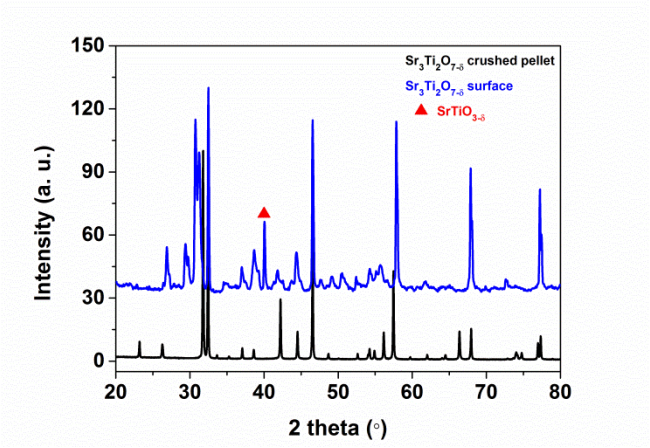


**Fig. 3.** XRD patterns of powder from a crushed $Sr_3Ti_2O_{7-\delta}$ pellet (lower) and its surface (upper) prior to crushing. The ceramic was sintered in 5% $H_2$ at 1773 K for 6 h.

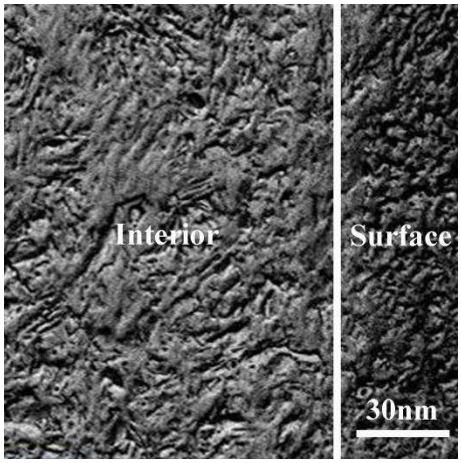


**Fig. 4.** Backscattered electron images on a cross section of $Sr_3Ti_2O_{7-\delta}$ ceramic sintered in 5% $H_2$.

**Table I. Relative percentage of Sr, Ti and the Sr/Ti ratio from the interior and surface regions of $Sr_3Ti_2O_{7-\delta}$ ceramic sintered in 5% $H_2$ at 1773 K. Theoretical values for $Sr_3Ti_2O_7$ are Sr = 60.00%, Ti = 40.00% with Sr/Ti = 1.50 and Sr = 50.00%, Ti = 50.00% with Sr/Ti = 1.00 for $SrTiO_3$.**

| Element | Bulk | | | Surface layer | | |
|---|---|---|---|---|---|---|
| | Sr L | Ti K | Sr/Ti | Sr L | Ti K | Sr/Ti |
| Relative % | 59.31 | 40.69 | 1.46 | 52.76 | 47.24 | 1.12 |
| | 62.08 | 37.92 | 1.64 | 52.14 | 47.86 | 1.09 |
| | 62.25 | 37.75 | 1.65 | 53.08 | 46.92 | 1.13 |
| | 62.61 | 37.39 | 1.67 | 53.37 | 46.63 | 1.14 |
| | 59.80 | 40.20 | 1.49 | 50.58 | 49.42 | 1.02 |
| | 60.98 | 39.02 | 1.56 | 49.88 | 50.12 | 1.00 |
| Average Relative % | 61.17 | 38.83 | 1.58 | 51.97 | 48.03 | 1.08 |

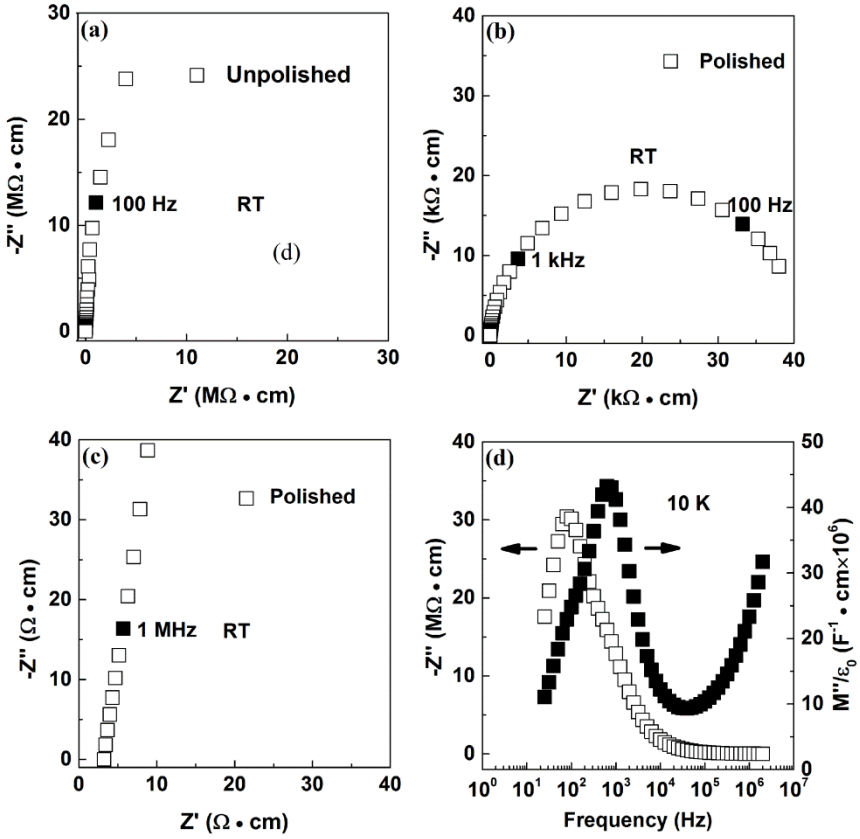


**Fig. 5.** Typical RT Z* plots of (a) an unpolished $Sr_3Ti_2O_{7-\delta}$ pellet, (b) a polished pellet, (c) inspection of high frequency data of (b); (d) combined -Z″ and M″ spectra of a polished $Sr_3Ti_2O_{7-\delta}$ pellet at 10 K, sintered in 5% $H_2$.

### (3) La-doped $Sr_3Ti_2O_{7-\delta}$ Ceramics Sintered in 5% $H_2$

The development of resistive surface layers on ceramics sintered in 5% $H_2$ also occurred in La-doped samples and was attributed (in part) to the uptake of oxygen during the post-sintering cooling process in 5% $H_2$. In an attempt to minimise the deleterious influence on σ [reverse reaction of mechanism (1)] for any re-oxidation on cooling, all ceramics

were prepared using a fast cooling rate of 30 $^{o}$C/min after sintering at 1773 K. Ceramics were then polished to ~50% of their original thickness prior to electrical measurements.

Powder samples of polished crushed pellets for the x-series compositions appeared single-phase by Laboratory XRD up to x = 0.05 with a simple cubic-type perovskite $SrTiO_{3-\delta}$ (ST) cell as an observable second phase in x = 0.10 sintered in 5% $H_2$, Fig. 1(a). XRD showed observable secondary phases including ST, $Sr_2TiO_4$ and $Sr_4Ti_3O_{10}$ for the y and z series (not shown).

The XRD patterns of the La-doped oxygen-deficient $Sr_3Ti_2O_{7-\delta}$ type phase in all samples were indexed on a tetragonal unit cell (space group I4/mmm) as reported in the literature[26]. For the x-series processed in 5% $H_2$, the lattice parameters and unit cell volume decreased smoothly with increasing x, Figs. 1(c) and (b), respectively therefore confirming the existence of a larger solid solution when compared to ceramics prepared in air.

TEM images of $(Sr_{1-x}La_x)_3Ti_2O_7$ (x = 0.01, 0.05) ceramics sintered in air and 5% $H_2$ obtained close to [110] are presented in Fig. 6. The [110] zone axis contains the (001) plane and thus reveals information about the SrO layers and any defects in the stacking sequence, particularly in samples that were tilted off-axis to give two beam bright field diffraction contrast conditions. Faint planar defects in these images represent essentially unstrained stacking faults in the RP superstructure, as shown in Figs. 6(c) for x = 0.01 processed in 5% $H_2$. Darker contrast planar defects were observed for x = 0.01 processed in air, Fig. 6(a) and arose because of deviations as a function of distance from a coherent Bragg condition and were associated with local lattice strain. Comparing Figs. 6(b) and (d) (x = 0.05, air and 5% $H_2$, respectively) the main difference is the clear formation of

discrete blocks of $SrTiO_3$ in air sintered samples interleaved between the RP phase. In contrast, the grains in x = 0.05 sintered in 5% $H_2$ remain essentially single-phase RP-type $Sr_3Ti_2O_7$.

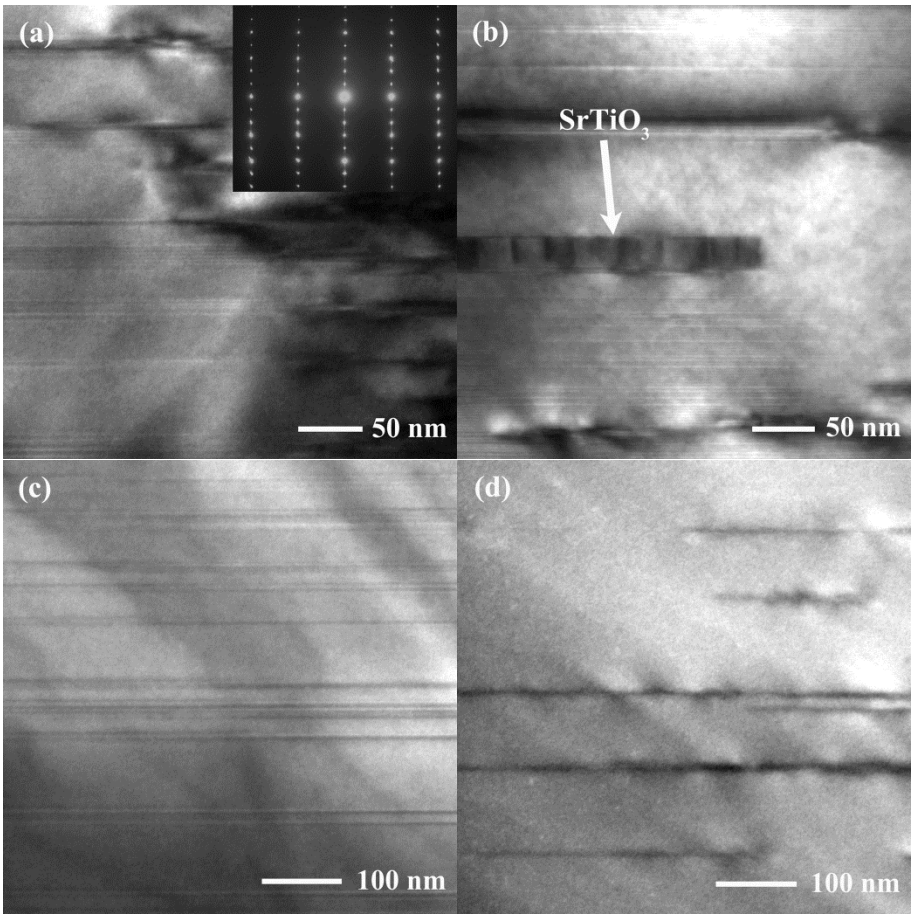


**Fig. 6.** Two-beam bright field TEM images of $(Sr_{1-x}La_x)_3Ti_2O_7$ samples obtained with the electron beam close to [110]. (a) x = 0.01 and (b) x = 0.05 sintered in air and (c) x = 0.01 and (d) x = 0.05 sintered in 5% $H_2$.

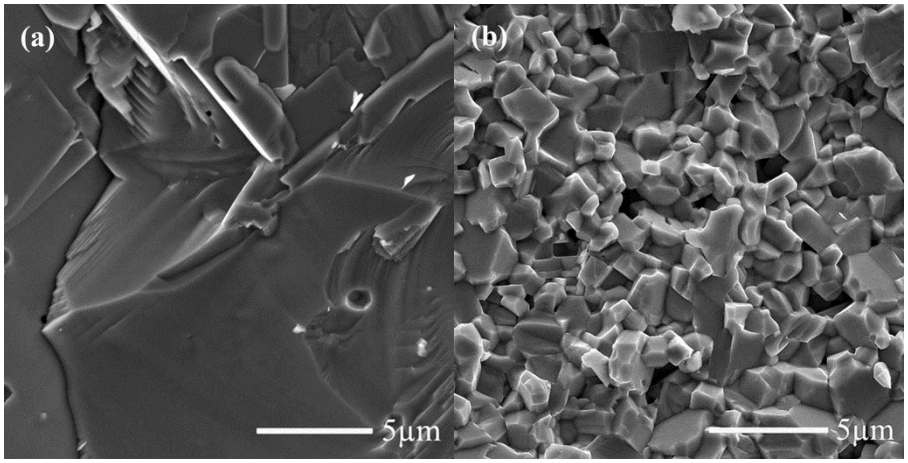


**Fig. 7.** Secondary electron images of a fractured surface for (a) x = 0.01 and (b) x = 0.05 ceramics sintered in 5% $H_2$.

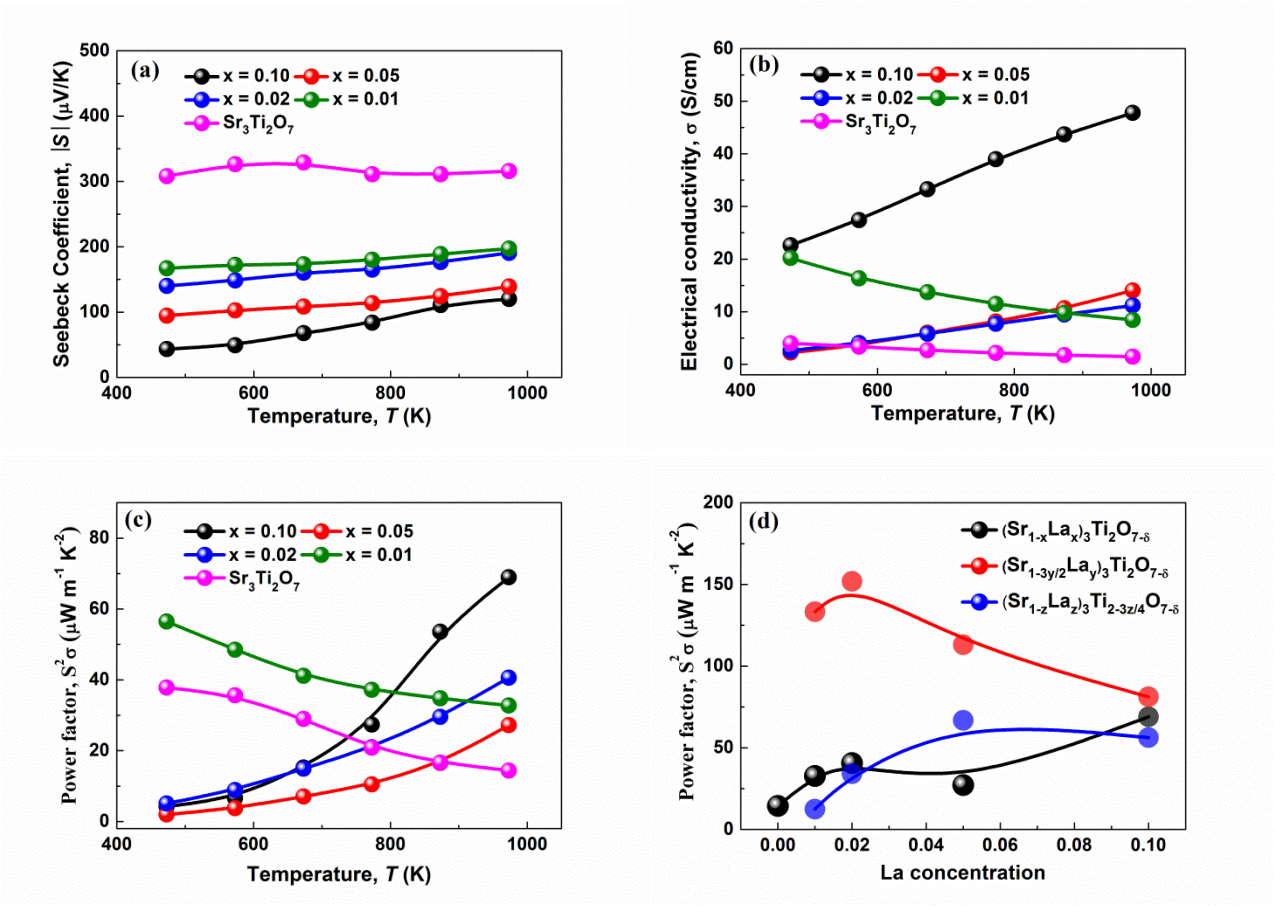

**Fig. 8.** Temperature dependence of (a) $|S|$, (b) $\sigma$, and (c) PF = $S^2\sigma$ for series x sintered in 5% $H_2$; (d) PF at 973 K versus La-content in $Sr_3Ti_2O_{7-\delta}$ ceramics sintered in 5% $H_2$ based on compositional series x, y and z.

Secondary electron images of fracture surfaces for x = 0.01 and 0.05 sintered in 5% $H_2$ showed the former to have a much larger average grain size compared to the latter, Fig. 7. The mechanism of grain growth under reducing conditions is not known at this juncture and is the subject of further study.

S values for all La-doped samples sintered in 5% $H_2$ were negative, suggesting all are n-type carriers. The absolute S value decreases with increasing x, Fig. 8(a) due to an increase in the carrier concentration, Fig. 8(b). Comparison of $\sigma$ at 973 K shows $\sigma$ to increase with x, however x = 0.01 shows metallic conduction whereas all other x values show semiconducting behaviour. The PF shows the same trend as $\sigma$ with temperature and reaches a maximum of ~70 $\mu W/m/K^2$ for x = 0.10 at ~973 K due to its high $\sigma$, Fig. 8(c). x = 0.10 contains the presence of a secondary ST phase, see Fig. 1(a), and this has a dramatic effect on the thermoelectric properties, Fig. 8(d). This observation made it prudent to measure the thermoelectric properties of ceramics from the other two series as they are phase mixtures by XRD that contain ST as a secondary phase, which implied higher power factors may be obtained in such ceramics, Fig. 8(d).

## IV. Discussion

XRD and TEM results show a very limited solid solution of La into $Sr_3Ti_2O_7$ for the x-series prepared in air with a small volume expansion in the unit cell of x = 0.01 compared to undoped $Sr_3Ti_2O_7$ (x = 0.00), Fig. 1(b). A larger solid solution with $x \leq 0.05$ appears to exist for samples processed under reducing conditions with an initial expansion of the unit volume for undoped $Sr_3Ti_2O_{7-\delta}$ (x = 0.00), followed by a systematic decrease with increasing x, Fig. 1(b). There was no appreciable solid solution for any y and z samples prepared in air or 5% $H_2$ at 1773 K.

These results show that creation of cation vacancies (A- or B-site) via La-doping, mechanisms, equation (3) and (4), respectively, are not favoured in RP-phases in air or reducing atmospheres which is in contrast to perovskite $SrTiO_3$ where a substantial solid solution containing A-site vacancies is known to exist[27]. All ceramics processed in air were white/yellow in appearance suggesting they were fully oxidised and IS showed all air sintered ceramics to be electrical insulators with low bulk conductivity and high $E_a$ (>1 eV), confirming electronic compensation, mechanism (2), does not exist for La-doping of ceramics sintered in air, Fig. 2. The lower bulk σ and higher $E_a$ of x = 0.01 samples compared to undoped $Sr_3Ti_2O_7$ ceramics confirms limited La-doping of the $Sr_3Ti_2O_7$ lattice does occur and that a change in conduction mechanism must also occur given the substantial increase in $E_a$ for x = 0.01, Fig. 2. $La^{3+}$ is a smaller ion than $Sr^{2+}$ so the observed increase in unit cell volume for x = 0.01 is attributed to the interstitial mechanism (5) that can occur in RP-type phases. The excess oxygen from the $La_2O_3$ may be associated with the interfaces between the RS layers and perovskite blocks in the RP

structure in the form of disordered defects and/or fill up any residual oxygen vacancies in the lattice due to acceptor impurities associated with the $TiO_2$ reagent[28]. The TEM image in Fig. 6(a) for x = 0.01 processed in air supports the idea of increased stain associated with the interstitial doping mechanism whereas the Arrhenius plot of bulk conductivity in Fig. 1 supports the change in conduction mechanism may be associated with a suppression of extrinsic (acceptor-type) conduction in undoped $Sr_3Ti_2O_7$ with an $E_a$ ~1.2 eV towards intrinsic conduction with $E_a$ >2 eV due to the filling up of extrinsic oxygen vacancies by the interstitial oxide ions. Unfortunately, the solid solution limit is low and it is not possible to unambiguously prove either (or both) of these possibilities.

Lattice parameters and cell volume obtained from XRD data of crushed powders from polished ceramics of the x series (including x = 0.00) sintered in 5% $H_2$, Figs. 1(b) and (c), reveal some interesting trends, especially when combined with the electrical conductivity results, Fig. 8 (b).

First, there is considerable expansion of the cell volume and a substantial increase in $\sigma$ when processing ceramics under reducing conditions when compared to those processed in air, as observed for both undoped (x = 0.00) and doped compositions (x = 0.01), Fig. 1(b). In the case of x = 0.00 this can be attributed solely to oxygen-loss with partial reduction of $Ti^{4+}$ to $Ti^{3+}$ ions based on Eq. (1). The ionic radius of $Ti^{3+}$ is 0.67 Å compared to 0.605 Å for $Ti^{4+}$ (for octahedral co-ordination) and this results in lattice expansion. The creation of oxygen vacancies can also result in lattice expansion due to a reduction in the Coulombic forces between the cations and anions in perovskites.[29] The green colour and significant $\sigma$ (~1 S/cm at 1000 K) for reduced x = 0.00 ceramics is consistent with the creation of mixed $Ti^{3+}/Ti^{4+}$ ions in the lattice whereas ceramics

processed in air are fully oxidized and insulating with only $Ti^{4+}$ ions in the lattice. In the case of x = 0.01, the larger unit cell volume of reduced ceramics compared to those processed in air can primarily be attributed to the creation of mixed $Ti^{3+}$, $Ti^{4+}$ content and this is consistent with an increase in σ.

Second, despite reduced ceramics containing larger $Ti^{3+}$ ions, cell volume decreases smoothly with increasing La-content for reduced La-doped samples, Fig. 1 (b). There is no systematic trend in σ with La-content; however, σ and therefore $Ti^{3+}$ content (based on the assumption that σ is dominated by carrier concentration as opposed to any changes in carrier mobility) is generally higher than that of reduced x = 0.00 and all are ~1 order of magnitude higher at 973 K, Fig. 8(b). This decrease in cell volume on La-doping is in contrast to the increase in cell volume observed for the La-doped x series processed in air, Fig. 1(b) and indicates the processing $pO_2$ influences the doping mechanism(s).

The increase in cell volume for x = 0.01 processed in air despite the smaller ionic radius of $La^{3+}$ compared to $Sr^{2+}$ was attributed to the interstitial doping mechanism [Eq. (5)] with incorporation of excess oxygen. Under reducing conditions, the most likely scenario is that donor doping [Eq. (2)] occurs as any interstitial oxygen ions are presumably more prone to removal under reduction compared with conventional lattice oxygen ions associated with the RP structure. Therefore, despite the production of larger $Ti^{3+}$ ions [Eq. (2)] and the possibility of creating oxygen vacancies under reducing conditions [Eq. (1)], unit cell volume contraction occurs due to the partial replacement of larger $Sr^{2+}$ with smaller $La^{3+}$ ions on the cation sublattice. It has previously been shown[13] that RE-dopants prefer the cation site associated with the RS layer compared to the

perovskite blocks in $Sr_3Ti_2O_7$ due to the lower co-ordination number of this site and the smaller ionic radius of RE-ions compared to Sr.

The electronic donor-doping compensation mechanism [Eq. (2)] is well known to occur in $SrTiO_3$ at low $pO_2$.[21,22] With increasing La doping level, the formation of local defect clusters in the matrix (maybe $La^{3+}$-O-$Ti^{3+}$) was observed by TEM along the [001] direction of the tetragonal cell, restricting grain growth and the average grain size as shown by SEM, Fig. 7. The TEM images also provide evidence about differences between series x samples sintered in air and 5% $H_2$. From this data, it is proposed that a reducing atmosphere not only encourages electronic compensation for $La^{3+}$ but may also be beneficial in releasing strain between the layers, thereby facilitating substitution into the Sr-sites of the RP $Sr_3Ti_2O_{7-\delta}$ phase and therefore extending the limit of the solid solution.

For x = 0.10, a simple perovskite-type '$SrTiO_{3-\delta}$' precipitates as an observable secondary phase, Fig. 1(a). The stoichiometry of the ST perovskite phase is unknown but is likely to be oxygen-deficient due to the reducing conditions and possibly contains La on the A-site and is therefore also A-site deficient. As discussed later, we propose this ST perovskite-phase to be more electrically conductive than the La-doped RP $Sr_3Ti_2O_{7-\delta}$ phase.

Processing in reducing conditions has a dramatic effect on undoped and La-doped $Sr_3Ti_2O_7$ ceramics. Sintering $Sr_3Ti_2O_7$ in 5% $H_2$ at 1773 K yields green coloured ceramics and is an effective method to strip oxygen (δ) based on Eq. (1) to induce semiconductivity in the interior of the ceramics, Fig. 5(c); however, this method also induces compositional changes on the ceramic surfaces. XRD on an unpolished ceramic

surface revealed the presence of $Sr_3Ti_2O_7$, a $SrTiO_3$-type phase and several unindexed peaks that could not be assigned to any known Sr-Ti-O phase(s) in the ICDD system, Fig. 3. A BEI of an unpolished ceramic from SEM revealed clear evidence of a surface layer, Fig. 4 and EDS analysis showed the surface to have a Sr/Ti ~1 compared to the expected value of ~1.5 observed from the interior of the ceramic, Table I. This change in phase assemblage and composition suggests some volatilization of Sr (possibly as SrO) in addition to oxygen-loss occurs from the ceramic surfaces under these reducing conditions at 1773 K. A combination of dense ceramics and higher surface diffusion of ions compared to bulk diffusion in these materials ensures outer pellet surfaces experience a lower local $pO_2$ compared to the pellet interiors and this introduces a $pO_2$ gradient within the ceramics. We propose this limits the level of SrO volatilization from the ceramic interiors (as they experience a higher local $pO_2$ compared to the outer surfaces) but the local $pO_2$ remains sufficient low to obtain a level of oxygen-loss ($\delta$) to induce semiconductivity in the RP $Sr_3Ti_2O_7$ phase. Although polished ceramics are single phase $Sr_3Ti_2O_{7-\delta}$ by XRD and TEM, the variation in local $pO_2$ experienced by these interior regions results in a heterogeneous distribution of the oxygen vacancies and the polished ceramics can be considered as being functionally graded.

IS at RT on an unpolished ceramic showed the presence of an insulating surface layer with R >10 MΩ, Fig. 5(a), that could be removed on polishing to reveal a non-ohmic electrode contact with R ~40 kΩ, Fig. 5(b), and a total ceramic resistivity of ~4 Ωcm, Fig. 5(c). Based on a combination of the XRD, SEM/EDS and IS results, we propose the insulating surface layer(s) on ceramics sintered under reducing conditions is associated with oxygen up-take and therefore oxidation of the reduced Sr-Ti-O phases at

the ceramic surfaces (including $SrTiO_3$ and $Sr_3Ti_2O_7$) during the cooling procedure after sintering.

All ceramics show negative S values, confirming n-type conduction consistent with mixed $Ti^{3+}$, $Ti^{4+}$ ions in the samples prepared under reducing conditions. Considering a temperature of 973 K to compare the thermoelectric properties, S drops by a factor of ~2-3 in series x up the solid solution limit of ~0.05 but the high temperature σ (at 973 K) has increased by ~1 order of magnitude (for all x) compared to x = 0.00. This shows the La doping mechanism has increased the carrier concentration, as all samples have been treated under the same reducing conditions so any conductivity due to oxygen-loss should be similar in all samples, irrespective of x. For electronic compensation [Eq. (2)], σ should increase systematically with x, however, x = 0.01, 0.02 and 0.05 all have similar σ at 973 K. In addition, x = 0.01 shows metallic temperature-dependent behaviour whereas 0.02 and 0.05 show semiconducting temperature-dependent behaviour, Fig. 8 (b), so the conduction mechanisms are different. The switch from metallic to semiconducting behaviour with increasing x may be related to extended defects/clusters/strain/grain boundary trapping of conduction electrons. For the single-phase samples in series x, the PF (at 973 K) has a dome shape with a maximum of ~40 $\mu W/m/K^2$ (for x ~0.02) that reflects the balance between a decrease in S with an increase in σ with increasing x, Fig. 8(d). This behaviour is consistent with the general observation that an increase in carrier concentration leads to a lower Seebeck coefficient[29].

It is interesting to consider the thermoelectric properties of x = 0.10 ceramics in series x as they contain secondary phases, including a cubic $SrTiO_{3-\delta}$ (ST)-type phase, Fig. 1(a). This has a dramatic effect on the thermoelectric properties. The σ is now a factor of

~50 higher than x = 0.00 and 5 times higher than x ~0.01-0.05 so clearly this secondary ST-type phase is more conductive than the RP phase. S drops for x = 0.10 ceramics as would be expected for its higher σ but this multi-phase ceramic has the highest PF for series x with a value of ~60 μW/m/K$^2$, Fig. 8(d). Series y and z are also multi-phase ceramics that contain a highly conducting ST-type phase. Generally, σ and S are higher in the y series compared to those in the x-series and as a consequence, PF values are substantially higher with y = 0.02 showing the highest value (~150 μW/m/K$^2$) of any ceramic, Fig. 8(d). A notable difference in the z series is the higher S values of z = 0.01 and 0.02 compared to the corresponding samples in the x and y series. This results in much higher PF values at lower temperatures in this series. At 973 K, z = 0.10 has the highest PF of this series with a value comparable to that of x = 0.10, Fig. 8(d). These results infer the cubic ST-type perovskite phase(s) have higher σ than any La-doped RP phase and therefore are more suitable for thermoelectric applications than RP phases.

## V. Conclusions

The La-doping mechanism in the RP-phase $Sr_3Ti_2O_7$ is dependent on the ceramic processing conditions. In air, a very limited oxygen interstitial mechanism [Eq. (5)] occurs with ceramics being electrically insulating whereas reducing conditions (e.g., 5% $H_2$ at 1773 K) are conducive towards electronic doping of La [Eq. (2)] and oxygen-loss [Eq. (1)] in $Sr_3Ti_2O_{7-\delta}$ ceramics. The heterogeneity of undoped and La-doped $Sr_3Ti_2O_7$ ceramics prepared under reducing conditions has a significant impact on the measured thermoelectric properties, especially with the development of resistive surface layers and

the presence of highly conducting secondary phases. Compared to $SrTiO_3$, σ of La-doped RP $Sr_3Ti_2O_{7-\delta}$ prepared under reducing conditions remain too low for the development of good thermoelectric properties at elevated temperatures, e.g., 973 K.

**Acknowledgements**

We thank the EPSRC for funding EP/L017563/1**.**

## References


[1]B. Poudel et al., "High-Thermoelectric Performance of Nanostructured Bismuth Antimony Telluride Bulk Alloys," Science, **320** [5876] 634-8 (2008).

[2]H. Goldsmid, "Bismuth Telluride and Its Alloys as Materials for Thermoelectric Generation," Materials, **7** [4] 2577-92 (2014).

[3]B. Yu, et al., "Enhancement of Thermoelectric Properties by Modulation-Doping in Silicon Germanium Alloy Nanocomposites," Nano Lett., **12** [4] 2077-82 (2012).

[4]D. Parker and D. J. Singh, "Potential Thermoelectric Performance from Optimization of Hole-Doped $Bi_2Se_3$," Phys. Rev. X, **1** [2] 021005, 9 pp (2011).

[5]K. Koumoto, Y. Wang, R. Zhang, A. Kosuga and R. Funahashi, "Oxide Thermoelectric Materials: A Nanostructuring Approach," Ann. Rev. Mater. Res., **40** [1] 363-94 (2010).

[6]J. He, Y. Liu and R. Funahashi, "Oxide Thermoelectrics: The Challenges, Progress, and Outlook," J. Mater. Res., **26** [15] 1762-72 (2011).

[7]M. Ohtaki, "Recent Aspects of Oxide Thermoelectric Materials for Power Generation from Mid-to-High Temperature Heat Source," J. Ceram. Soc. Jpn., **119** [11] 770-75 (2011).

[8]H. Muta, K. Kurosaki and S. Yamanaka, "Thermoelectric Properties of Reduced and La-Doped Single-Crystalline $SrTiO_3$," J. Alloys Compd., **392** [1-2] 306-9 (2005).

[9]S. Ohta, T. Nomura, H. Ohta, M. Hirano, H. Hosono and K. Koumoto, "Large Thermoelectric Performance of Heavily Nb-doped $SrTiO_3$ Epitaxial Film at High Temperature," Appl. Phys. Lett., **87** [9] 092108, 3pp (2005).

[10]S. Ohta, T. Nomura, H. Ohta and K. Koumoto, "High-Temperature Carrier Transport and Thermoelectric Properties of Heavily La- or Nb-Doped $SrTiO_3$ Single Crystals," J. Appl. Phys., **97** [3] 034106, 4pp (2005).

[11]K. H. Lee, S. W. Kim, H. Ohta and K. Koumoto, "Ruddlesden-Popper Phases as Thermoelectric Oxides: Nb-doped $SrO(SrTiO_3)_n$ (n=1,2)," J. Appl. Phys., **100** [6] 063717, 7pp (2006).

[12]K. H. Lee, Y. F. Wang, S. W. Kim, H. Ohta and K. Koumoto, "Thermoelectric Properties of Ruddlesden-Popper Phase n-Type Semiconducting Oxides La-, Nd-, and Nb-Doped $Sr_3Ti_2O_7$," Int. J. Appl. Ceram. Tec., **4** [4] 326-31 (2007).

[13]Y. F. Wang, K. H. Lee, H. Ohta and K. Koumoto, "Fabrication and Thermoelectric Properties of Heavily Rare-Earth Metal-Doped $SrO(SrTiO_3)_n$ (n = 1, 2) ceramics," Ceram. Int., **34** [4] 849-52 (2008).

[14]Y. Wang, K. H. Lee, H. Hyuga, H. Kita, H. Ohta and K. Koumoto, "Enhancement of Thermoelectric Performance in Rare Earth-Doped $Sr_3Ti_2O_7$ by Symmetry Restoration of $TiO_6$ Octahedra," J. Electroceram., **24** [2] 76-82 (2008).

[15]Y. Wang, K. H. Lee, H. Ohta and K. Koumoto, "Thermoelectric Properties of Electron Doped $SrO(SrTiO_3)_n$ (n = 1,2) Ceramics," J. Appl. Phys., **105** [10] 103701, 6pp (2009).

[16]N. Sirikanda, H. Matsumoto and T. Ishihara, "Effects of Rock-Salt Layer on Electronic and Oxide Ionic Mixed Conductivity in Strontium Titanate, $SrO(SrTiO_3)_n$ (n=1, 2, $\infty$)," Solid State Ionics, **181** [5-7] 315-21 (2010).

[17]J. Liu, et al., "Enhancement of Thermoelectric Efficiency in Oxygen-Deficient $Sr_{1-x}La_xTiO_{3-\delta}$ Ceramics," Appl. Phys. Lett., **95** [16] 162110, 3pp (2009).
[18]J. Ravichandran, et al., "High-Temperature Thermoelectric Response of Double-Doped $SrTiO_3$ Epitaxial Films," Phys. Rev. B, **82** [16] 165126, 5 pp (2010).
[19]A. Kikuchi, N. Okinaka and T. Akiyama, "A Large Thermoelectric Figure of Merit of La-Doped $SrTiO_3$ Prepared by Combustion Synthesis with Post-Spark Plasma Sintering," Scripta Mater., **63** [4] 407-10 (2010).
[20]N. G. Eror and U. Balachandran, "Self-Compensation in Lanthanum-Doped Strontium Titanate," J. Solid State Chem., **40** [1] 85-91 (1981).
[21]U. Balachandran and N. G. Eror, "Electrical Conductivity in Lanthanum-Doped Strontium Titanate," J. Electrochem. Soc., **129** [5] 1021-6 (1982).
[22]B. F. Flandermeyer, A. K. Agarwal, H. U. Anderson and M. M. Nasrallah, "Oxidation-Reduction Behaviour of La-Doped $SrTiO_3$," J. Mater. Sci., **19** [8] 2593-8 (1984).
[23]C. Navas, H. L. Tuller and H. zur Loye, "Electrical Conductivity and Nonstoichiometry in Doped $Sr_3Ti_2O_7$," J. Eur. Ceram. Soc., **19** [6-7] 737-40 (1999).
[24]D. C. Sinclair and A. R. West, "Bulk PTCR Effect on Doped $BaTiO_3$," J. Mater. Sci. Lett., **7** [8] 823-4 (1988).
[25]D. C. Sinclair and A. R. West, "Impedance and Modulus Spectroscopy of Semiconducting $BaTiO_3$ Showing Positive Temperature Coefficient of Resistance," J. Appl. Phys., **66** [8] 3850-6 (1989).
[26]S. N. Ruddlesden and P. Popper, "The Compound $Sr_3Ti_2O_7$ and its Structure," Acta Crystallogr., **11**, 54-5 (1958).
[27]A. D. Aljaberi and J. T. S. Irvine, "Ca-Substituted, A-Site Deficient Perovskite $La_{0.2}Sr_{0.7}TiO_3$ as a Potential Anode Material for SOFCs," J. Mater. Chem. A, **1** [19] 5868-74 (2013).
[28]N.-H. Chan, R. K. Sharma and D. M. Smyth, "Nonstoichiometry in Acceptor-Doped $BaTiO_3$," J. Am. Ceram. Soc., **65** [3] 167-70 (1982).
[29]M. Cutler, J. Leavy and R. Fitzpatrick, "Electronic Transport in Semimetallic Cerium Sulfide," Physical Review, **133** [4A] A1143-52 (1964).